Analytical Methods

ROYAL SOCIETY OF CHEMISTRY

PAPER

View Article Online
View Journal | View Issue

Cite this: *Anal. Methods*, 2024, **16**, 742

An impedimetric sensor based on molecularly imprinted nanoparticles for the determination of trypsin in artificial matrices – towards point-of-care diagnostics†

Sabrina Di Masi, ‡*[a] Marco Costa,[a] Francesco Canfarotta,‡*[b] Antonio Guerreiro,[b] Alicia Hartley,[b] Sergey A. Piletsky[c] and Cosimino Malitesta[a]

Received 5th October 2023
Accepted 28th December 2023

DOI: 10.1039/d3ay01762a

rsc.li/methods

A high-performance impedimetric sensing platform was designed to detect proteins by employing molecularly imprinted polymeric nanoparticles (nanoMIPs) as selective receptors. This was achieved *via* the combination of the nanoMIPs with a self-assembled thioctic acid (SAM-TA) monolayer onto screen-printed gold electrodes, providing stable covalent attachment of the selective binder to the transducer. Taguchi design has been modelled to achieve the optimal level of sensor fabrication parameters and to maximise the immobilisation of nanoMIPs and their response (*e.g.* the response of imprinted polymers compared with the non-imprinted control). The developed sensor was tested towards a range of concentrations of trypsin dissolved in ammonium acetate (pH = 6) and showed promising applicability in artificial saliva, with a recovery percentage between 103 and 107%.

1. Introduction

Trypsin and pepsin are two proteases that are considered biomarkers for some diseases connected with the gastrointestinal tract. For instance, pepsin can be detected in saliva and it is currently used in diagnostics as a biomarker for gastro-esophageal reflux disease.[1] Trypsin, on the other hand, is considered a biomarker of pancreatic cancer (PC), which is a highly aggressive cancer that still accounts for more than 7% of deaths among patients worldwide.[2,3] PC often remains undetected until the late stages of the disease, which makes early detection a challenge. Specific biomarkers, such as serine-proteases have been reported as disease biomarkers for the diagnostics of PC.[4] Hence, trypsin (Ty) has been recognised as a biomarker to be detected in a non-invasive way in biological samples.[5,6] Typically, clinical trypsin concentration in serum samples ranges between 5 and 15 nM for healthy individuals, whereas the increased concentration at 34–85 nM can reveal a pancreatic condition.[7,8] Therefore, detection of trypsin and its quantification in biological samples is still highly relevant.

Currently, most of the screening tools for cancer diagnosis still remain highly invasive, requiring expert teams and very expensive methods.[9] At the same time, non-invasive analysis is not often available for the vast majority of cancer types, and the specificity of diagnostics is insufficient to allow routine screening of specific biomarkers. On the other hand, oral fluids *e.g.* human saliva, can be considered the ultimate body fluid for the non-invasive examination. Most importantly, despite the dissimilarities between oral fluids and whole blood, the distribution of biological processes, cellular components and molecular function is comparable.[10]

Hence, point-of-care (POC) systems still need accurate screening tests with high sensitivity and selectivity to detect very low signal changes. Electrochemical sensors can meet POC requirements since they provide rapid, non-invasive, simple screening tools.[11,12] Molecularly imprinted polymers (MIPs) as selective receptors have been widely employed for sensor development,[13–17] thanks to their remarkable molecular recognition properties, chemical stability, low cost of manufacturing and stability. These synthetic materials are prepared by template-directed polymerization and possess binding motifs selective for a specific target (the template). MIPs can be prepared in a variety of formats, from monoliths and membranes to nanoparticles (nanoMIPs). The latter can easily be attached to electrode surfaces[18–20] and fulfil the requirements for accurate sensing in clinical settings.[21,22]

A key step in the development of a sensing platform is the immobilization of the selective receptor onto the electrode. One of the commonly used methods is the modification of gold

[a]*Laboratorio di Chimica Analitica, DiSTeBA, Università del Salento, Edificio A6, Via per Monteroni, 73100, Lecce, Italy. E-mail: sabrina.dimasi@unisalento.it*

[b]*MIP Discovery, Colworth Park, Sharnbrook, MK44 1LQ Bedford, UK. E-mail: Francesco.Canfarotta@mipdiscovery.com*

[c]*Department of Chemistry, University of Leicester, University Rd, LE1 7RH Leicester, UK*

† Electronic supplementary information (ESI) available. See DOI: https://doi.org/10.1039/d3ay01762a

‡ These authors contributed equally to this work.

electrode surfaces *via* self-assembled monolayers (SAMs) using carboxyl-terminated linkers.[23,24] Therefore, the receptors can be easily immobilized by activation of carboxyl groups through carbodiimide chemistry. Thioctic acid (TA) is a ligand which has been previously used for modification of gold nanoparticles and their subsequent linkage to proteins.[25] Facile preparation of a redox-active thioctic acid-based SAM on gold electrodes can be carried out either by chemical adsorption (most common approach) or electrochemically,[26,27] at moderate cathodic potentials (−0.4 V *vs.* SCE).

With the aim of developing a new monitoring platform for Ty with good selectivity/sensitivity and fast response, we propose an electrochemical sensor combining nanoMIPs as the receptor, with a TA-SAM functionalised screen-printed gold electrode (SPAuE) as the transducer. As mentioned above, saliva is the biological fluid of choice for non-invasive sampling. In order to assess the feasibility of a nanoMIP-based sensor that can perform in biological fluids, artificial saliva was selected as a model sample matrix. The nanoMIPs were prepared by following two strategies: liquid-phase polymerisation[28] and solid-phase polymerisation.[29] To design the sensor, an optimisation method based on multivariate design of experiment (DoE) was explored, aimed at maximising the recognition qualities of nanoMIPs. The application of the developed sensor provides a promising perspective on the quantification of Ty protein in artificial biological samples with low cross-reactivity compared to co-existing interferents, such as mucin and pepsin.

2. Experimental section

2.1 Materials

Acrylamide, ammonium persulfate, trypsin, pepsin, and mucin, absolute ethanol, toluene, sodium phosphate dibasic, *N*-hydroxysuccinimide (NHS), *N*-(3-dimethylaminopropyl)-*N*′-ethylcarbodiimide hydrochloride (EDC), *N*,*N*′-methylenebisacrylamide (BIS), *N*-(3-aminopropyl)methacrylamide hydrochloride (APMA), *N*,*N*,*N*′,*N*′-tetramethylethylenediamine (TEMED), (3-aminopropyl) triethoxysilane (APTES), *tert*-butyl acrylate (TBAC), mercaptoundecanol, mercaptoundecanoic acid, methacrylic acid, sodium dodecyl sulphate, ethylene glycol dimethacrylate (EGDMA) glutaric dialdehyde (50% solution) and Amicon® ultra-15 centrifugal filters (30 kDa MWCO) were all purchased from Merck (Gillingham, UK). Thioctic acid (α-lipoic acid) and ammonium acetate were purchased from Merck (Milan, Italy). Phosphate buffered saline (PBS, 10× concentration) and Snakeskin® dialysis membranes were purchased from Fisher Scientific (Loughborough, UK). Sodium phosphate monobasic monohydrate and sodium phosphate dibasic heptahydrate were obtained from Fisher Scientific Italia (Rodano, Italy) to prepare the PBS 50 mM, pH 6. Bovine serum albumin was from Jackson ImmunoResearch (West Grove, USA). Glass beads with a diameter between 50 and 105 μm were from Microbeads AG (Gebenstorf, Switzerland). Thioctic acid solution was prepared in absolute ethanol (3 mg mL^{-1}). All materials were used as received; type I water was used throughout the experiments. Ammonium acetate buffer (50 mM, pH 6) was used to prepare trypsin stock solutions and the subsequent dilutions.

2.2 Preparation of trypsin imprinted polymers (Ty-nanoMIPs) and non-imprinted polymers (nanoNIPs)

2.2.1 Synthesis by liquid phase polymerisation (SOL-Ty-nanoMIPs and nanoNIPs). The synthetic procedure was adapted from ref. 30. To 200 mL of phosphate buffer (20 mM concentration, pH 7.4) 0.04 g SDS was added. The SDS-phosphate buffer was then used to prepare a monomer stock solution containing the following: 160 mg BIS, 4 μL EGDMA, 9.8 μL methacrylic acid, 8 mg acrylamide, 7.2 μL *tert*-butyl acrylate, and 2.4 mg APMA. The stock solution was then divided into two 100 mL fractions and added to 100 mL glass bottles. To prepare the MIP, 3 mg of trypsin were added to one of the bottles, and control (non-imprinted polymers, NIPs) was prepared in the absence of trypsin. The solutions were then degassed under vacuum and sonicated for 5 min. To initiate polymerisation, 40 mg APS dissolved in 250 μL water was added to each bottle, followed by 38 μL of TEMED. Immediately after the addition of the initiator the headspace was flushed with nitrogen and the bottle was capped; polymerisation was carried out for 12 h. After polymerisation, the solutions containing polymer nanoparticles were filtered through a 0.45 μm PVDF syringe filter followed by concentration down to 1 mL using 30 kDa MWCO centrifugal filters. To remove unreacted monomers, template, and buffer components both polymers were further washed on the centrifugal filter once with 15 mL of 10× PBS and ten times with 15 mL water. After washing, both the MIP and NIP were re-suspended in 2 mL water and stored at 4 °C until use.

2.2.2 Synthesis by solid phase polymerisation (SP-Ty-nanoMIP). The synthetic procedure was adapted from ref. 31. Glass beads (acting as a solid-phase) were first activated by boiling in a 4 M NaOH solution for 15 min, then washed with deionized water until neutral pH and rinsed with acetone, dried at 80 °C and subsequently incubated overnight in 2% v/v APTMS in dry toluene solution (0.4 mL solution per g glass beads). For the immobilisation of trypsin onto the solid phase, APTMS-derivatised glass beads were first incubated in 7% (v/v) glutaraldehyde solution in PBS for 2 h. Afterwards, the beads were placed in a bottle containing a solution of trypsin in PBS (1 mg mL^{-1}, 0.4 mL solution per g glass beads) and incubated overnight at 4 °C. After overnight incubation, the beads were washed with water using a sintered funnel. For the synthesis of SP-Ty-nanoMIPs, the following monomers and cross-linkers were dissolved in water (100 mL): acrylamide (24 mg), BIS (6 mg), acrylic acid (2.2 μL), TBAC (38 μL), APMA (6 mg). The monomer solution was degassed under vacuum and sonicated for 5 min, and then bubbled with N_2 for 4 min. Then, 60 g of trypsin-derivatised glass beads were added to the solution. Polymerisation was initiated by adding freshly prepared ammonium persulfate in aqueous solution (0.5 mL, 120 mg mL^{-1}) followed by TEMED (30 μL). Polymerization was carried out at room temperature for 45 min. Subsequently, the content of the polymerization vessel was poured into a solid-phase extraction cartridge (60 mL) equipped with a frit (20 μm porosity). A total of eight washes with 20 mL of water at 20 °C were carried out to remove low affinity polymers, oligomers and unreacted monomers. Afterwards, 20 mL of ethanol were added to the SPE

cartridge containing the solid phase. The cartridge was then placed in a water bath at 70 °C for 15 min and the hot ethanol fraction was eluted under vacuum. A total of four washes at 70 °C were performed. The collected ethanol washes were combined and then filtered through a PVDF 0.45 μm syringe filter and evaporated down to approximately 15 mL. The ethanolic nanoMIP solution was dialysed at 45 °C for 24 h against 5 L water using a 10 kDa MWCO regenerated cellulose membrane.

2.3 Characterisation of Ty-nanoMIPs

The size of the nanoparticles was determined by dynamic light scattering (DLS) with a Zetasizer Nano (Malvern Instruments Ltd, UK). Morphological analysis by transmission electron microscopy (TEM) was performed using JEOL JEM-1400 TEM with an accelerating voltage of 120 kV. Images were captured using an EMSIS Xarosa 20 MP digital camera with Radius software. The grids were plasma discharged at 30 mA for 15 seconds to create a hydrophilic surface. A 5 μL drop of an aqueous solution of nanoparticles was placed on a surface treated grid for 3 min and then the excess dispersion was removed using filter paper. Then a 2 μL drop of a 0.1% w/v aqueous solution of uranyl formate (negative stain) was added to the grid loaded with the sample for 30 seconds and the excess stain was removed using a tissue paper filter. The interactions between trypsin and MIP nanoparticles were assessed using a Biacore 3000 SPR instrument (Cytiva, UK). Au-coated chips (SIA Kit Au, Cytiva, UK) were cleaned with plasma using air as process gas on an HPT 100 plasma cleaner (Enniken Plasma, UK). The sensor chips were then coated by immersion in an ethanol solution containing mercaptoundecanoic acid (0.009 mg mL^{-1}) and mercaptoundecanol (0.19 mg mL^{-1}) for 24 h. Chip surface activation was performed online by injecting at a flow rate of 10 μL min^{-1} 0.1 mL of aqueous solution of EDC and NHS at 20 and 6 mg mL^{-1}, respectively. Immediately after activation, trypsin (1 mg mL^{-1}) in PBS pH 7.4 was injected at 10 μL min^{-1}, 0.1 mL injection volume. Control channels were modified by injecting a control protein (BSA) under similar conditions to the trypsin. All binding affinity experiments were performed in PBS, pH 7.4 at 25 °C and a flow rate of 50 μL min^{-1}. For this, 80 μL aliquots of nanoMIPs were injected, with 2 min dissociation time. Kinetic data were fitted using BIAevaluation software v. 4.1 (GE Healthcare Life Sciences, UK).

2.4 Sensor preparation

2.4.1 SAM of thioctic acid (TA-SAM) onto gold screen-printed electrodes. Disposable screen-printed gold electrodes (SPAuE, DRP-220AT, Metrohm, Italy) were used as the transduction element for sensor development. They consisted of a gold disk-shaped (12.6 mm^2) working electrode, a gold strip counter electrode, and a paste of silver reference electrode on a ceramic substrate (3.3 cm × 1.0 cm). First, the electrode (SPAuE) was rinsed with water to remove impurities. Then, thiol SAMs were formed using a thioctic acid (TA) solution. The solution was prepared in absolute ethanol. To allow formation of the self-assembled monolayer, the clean SPAuEs were subjected to (i) overnight incubation at 4 °C (obtaining o-TA-SAM) and (ii) chronoamperometric analysis (CA, obtaining e-TA-SAM) at − 0.35 V (*vs.* Ag reference) for variable time, in 3 mL of TA solution (3 mg mL^{-1}). Afterwards, the TA-SAMs onto SPAuE were rinsed with absolute ethanol and water, and ready for further use.

2.4.2 Nanoparticle immobilisation. Prior to the immobilisation step, the stock solution of nanoMIPs (and related diluted solutions) was sonicated for 2 min, to avoid possible aggregation. For the sensor preparation, both the thiol activation of TA-SAM and nanoMIP/nanoNIP immobilisation were performed by using carbodiimide chemistry. For this, the TA-SAM/SPAuE was wetted with a drop (100 μL) of PBS (0.1 mol L^{-1}, pH 7.4) containing 50 μL of nanoMIPs (or nanoNIPs), 25 μL of EDC (30 mM), and 25 μL of NHS (60 mM), for variable time (see Scheme S1†). This way the sensing platform was obtained, hereafter denoted as the Ty-nanoMIP sensor. Both nanoMIPs were immobilised onto TA-SAM/SPAuE, thus obtaining the SOL-Ty-nanoMIP and SP-Ty-nanoMIP sensors, respectively. Corresponding NIP sensors have been obtained by following the same procedure. The sensors were stored in ammonium acetate solution (50 mM, pH = 6) at 4 °C when not in use.

2.4.3 Optimisation of sensor preparation. To evaluate the optimum conditions for sensor preparation, three main parameters have been selected and studied in an orthogonal array experimental design (Taguchi design). Specifically, the effects of (i) chronoamperometric deposition time, (ii) the nanoparticle immobilisation time, and (iii) the analyte loading time have been ranged in three levels, obtaining a L9 (3 × 3) array (Table S1 in the ESI†). The experimental design was carried out following the criterion "larger-the-best", with respect to maximising the responses of the nanoMIPs compared to nanoNIPs. The difference in the observed charge transfer resistance (ΔR_{ct}) – after the exposure to 3 ng per mL trypsin – was assigned as the response (Y) of the experiments. Each experiment was repeated four times, and the average responses were calculated. To observe the quality characteristics of the imprinted polymer, the imprinting factors (IF) (eqn (1)) were calculated for each experiment. The signal-to-noise ratio (S/N ratio) of the IF was used to indicate the magnitude of changes in responses to variations in controlled parameters with respect to errors.[32]

$$\mathrm{IF} = \frac{\Delta R_{ct}\ \text{nanoMIP}}{\Delta R_{ct}\ \text{nanoNIP}}; \quad \text{where } \Delta R_{ct} = R_{ct}\left(3\ \text{ng mL}^{-1}\right) - R_{ct}(0) \tag{1}$$

Minitab® (version 18.1) was used for DoE analysis of results.

2.5 Electrochemical characterisation of sensors

The developed sensors were characterised by electrochemical impedance spectroscopy (EIS) measurements by comparing results for each stage of modification. Basically, the electrochemical measurements on bare SPAuE, the TA-SAM/SPAuE and Ty-nanoMIPs/nanoNIP sensors have been conducted in the solution of 0.1 M KCl containing 10 mM $Fe(CN)_6^{3-/4-}$ as the electrochemical redox probe. EIS analysis was carried out in the frequency range from 100 kHz to 0.1 Hz, at E_{ac} of 20 mV and E_{dc} of +0.23 V (*vs.*

Ag reference). The impedance spectra were fitted and interpreted using a Randles equivalent circuit (see Fig. S1 in the ESI†).

2.6 Analytical assessment and kinetic studies of Ty-nanoMIP sensors

Preliminary tests were performed by comparing the analytical assessment on SP-Ty-nanoMIP and SOL-Ty-nanoMIP sensors towards increased concentration of Ty. Therefore, the best-performing sensor was chosen for further optimisation and characterisation studies. The analytical performances of the optimised sensors have been performed in a standard solution of ammonium acetate at pH = 6, in the presence of varying concentrations of trypsin, from 3 ng mL^{-1} to 46 ng mL^{-1}. EIS measurements were carried out in the presence of PBS (0.05 M, pH = 6) containing 10 mM $Fe(CN)_6^{3-/4-}$ as the electrochemical redox probe, in the frequency range from 100 kHz to 0.1 Hz, E_{dc} = +0.23 V (*vs.* Ag reference), and E_{ac} = 0.02 V. The protocol to obtain the sensor responses comprised:[1] Ty-nanoMIP sensor was incubated in a blank solution (ammonium acetate) for variable time;[2] a drop of 100 μL of the redox probe was deposited on the electrode surface;[3] EIS spectra were recorded;[4] Ty-nanoMIP sensor was rinsed with ammonium acetate;[5] Ty-nanoMIP sensor was again exposed to the next Ty concentration. The analytical quantification of Ty in Ty-nanoMIP sensors took 3 min to be completed. EIS sensor responses ($\Delta R_{ct} = R_{ct}$ after [Ty] − R_{ct} after blank exposure) were recorded and used for calibration plots. Basically, sensor responses were followed by monitoring the changes in charge transfer resistance (R_{ct}) of the redox probe ($[Fe(CN)_6]^{3-/4-}$ ions) after exposure to Ty tested concentration. Using this approach, it was assumed that the rebinding of template molecules should reveal cavities that enable lower diffusion of the probe leading to a corresponding decrease in charge transfer (*i.e.* an increase in charge transfer resistance, R_{ct}) between the underlying SPAuE gold substrate and the ionic species of the redox probe. The limit of detection (LOD) was calculated as $3 \times s/m$, where s is the standard deviation of the intercept and m is the slope of the regression plot.

Kinetic binding isotherms of the sensor, and related kinetic parameters, were obtained and calculated using OriginPro 2016 software. The Temkin isotherm function[33] was selected for experimental sensor data fitting.

2.7 Electrochemical evaluation in artificial saliva

After the analytical assessment in ammonium acetate buffer solution, the performance of the developed sensors was assessed in artificial saliva, which has a similar electrolyte concentration to human saliva.[34] The artificial saliva was prepared as reported elsewhere,[35] and spiked with trypsin (150 ng mL^{-1}, stock solution) then diluted down with additional artificial saliva to obtain the desired trypsin concentration. Recovery percentages (%) were then calculated and reported.

3. Results and discussion

3.1 Characterisation of the nanoparticles

The hydrodynamic size of SOL-Ty-nanoMIPs and SP-Ty-nanoMIPs was determined by DLS measurement (Fig. S2 in the ESI†). The results showed a diameter of 15.3 ± 0.3 nm (n = 3) for SOL-Ty-nanoMIPs and 74.1 ± 0.5 nm (n = 3) for SP-Ty-nanoMIPs at 25 °C, respectively. The morphology of nanoparticles was evaluated by TEM analysis (Fig. S3 in the ESI†). As shown, the SOL-Ty-nanoMIPs and SP-Ty-nanoMIPs exhibited different sizes and distributions. Specifically, the SP-Ty-nanoMIPs appeared more spherical than SOL-Ty-nanoMIPs and presented a more homogeneous size distribution. This can be explained by the presence of the solid phase support during the nanoMIP production since it allows for affinity purification of the obtained nanoparticles, and this step removes also irregular materials formed in solution.[29] SOL-nanoMIPs tend to aggregate, as visible from their related TEM images. In order to evaluate the dissociation constant (K_D) of the proposed nanoMIPs, SPR analysis was performed and sensorgrams were shown below (Fig. 1). The real-time binding analysis confirmed the attachment of the nanoMIPs to the surface of the sensor chip coated with trypsin and a cumulative concentration assay was performed by injecting increasing concentrations of nanoMIPs (from 0.07 pM to 0.3 nM) suspended in PBS pH 7.4; reference channels derivatised with BSA were used as controls.

Sensorgrams for both synthesised nanoMIPs confirmed the high affinities towards trypsin with dissociation constants (K_D)

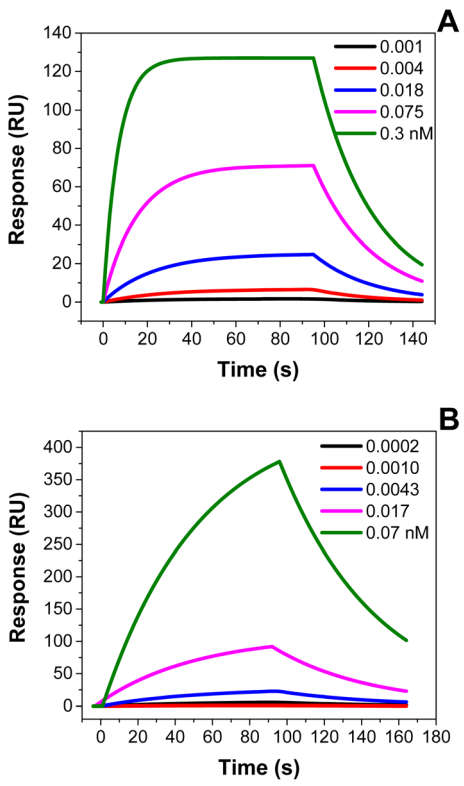

Fig. 1 SPR sensorgrams for (A) SOL-Ty-nanoMIPs and (B) SP-Ty-nanoMIPs injected onto immobilised trypsin. Carboxyl-derivatised SPR chips were modified with either trypsin or BSA by injection of EDC/NHS followed by the proteins in PBS pH 7.4, as recommended by the manufacturer. NanoMIP injections were performed in PBS pH 7.4. Five injections (with 1 : 4 dilutions) were performed with a concentration range from 0.07 pM to 0.3 nM. Data were fitted with the BiaEvaluation software 4.1 (GE Healthcare) using a 1 : 1 Langmuir binding model.

calculated as 38 nM and 11 nM, for SOL-Ty-nanoMIPs and SP-Ty-nanoMIPs, respectively. Nevertheless, the SP-Ty-nanoMIPs show a slightly higher affinity to the target because of their manufacturing process: it is a well known fact that solid-phase imprinting tends to produce nanoMIPs with better affinity, probably due to the consistent presentation of the template molecule on the solid-phase (as opposed to when the template is free in solution).

3.2 Sensor preparation

3.2.1 Preparation and electrochemical characterisation of TA-SAMs/SPAuE. For functionalization of SPAuEs surfaces, TA-SAMs were prepared by (i) classical incubation (o-TA-SAM), and by (ii) chronoamperometry (e-TA-SAM) at −0.35 V (2500 s) in TA ethanolic solution (3 mg mL^{-1}). Afterwards, TA-SAMs/SPAuE were subjected to nanoMIP immobilisation (45 min) for sensor development. Initially, cyclic voltammetry (CV) measurements were performed to evaluate electrochemistry at the SPAuEs after each modification. Each CV differs not significantly in current density (data not shown). Therefore, EIS measurements in the redox probe of $Fe(CN)_6^{3-/4-}$ were carried out to monitor the outcome of modifications onto SPAuEs surfaces, as well as the immobilisation of nanoMIPs on each prepared TA-SAM (Fig. S4 in the ESI†). The R_{ct} value of bare SPAuE was 757 Ω. Immersion in 3 mg per mL TA overnight generated increased resistance at 9343 Ω for o-TA-SAM and 1.57 × 10^4 Ω for e-TA-SAM, respectively. This increase in the interfacial electron transfer can be explained by the presence of the SAM layers that hinders the electron transfer at both electrode surfaces. The assembly of nanoMIPs onto TA-SAMs generated a tightly packed MIP layer that introduced a barrier to the interfacial electron transfer, which is clearly indicated by the increase of R_{ct} of the TA-SAMs (9582 Ω for o-TA-SAM and 1.99 × 10^4 Ω for e-TA-SAM, respectively). However, nanoMIP immobilisation resulted in more pronounced e-TA-SAM. This result clearly demonstrates the intimate differences of the obtained TA-SAMs onto SPAuE: in fact, it was already reported that the formation of thiol-based SAMs under controlled potential can lead to effective and reproducible coverage of gold electrode surfaces compared to the conventional passive adsorption.[26] Therefore, the e-TA-SAM was chosen for functionalization of SPAuE surfaces and further considered for sensor development.

3.2.2 Preliminary tests on nanoMIP selection. After the evaluation of binding affinities of the synthesised nanoMIPs, the same were deposited onto TA-SAM and tested towards increased concentration of Ty (3, 6, 12, 27, and 46 ng mL^{-1}) dissolved in ammonium acetate (50 mM, pH 6) (see Fig. S5 in the ESI†). For the preliminary test, sensors were prepared by CA measurement at −0.35 V (2500 s) for TA-SAM preparation, and 45 min for nanoMIP immobilisation at a concentration of 1 mg mL^{-1}. EIS data comparison and obtained calibration curves are shown in Fig. S5 in the ESI.† Experimental data were fitted with kinetics described by the Temkin isotherm, as already reported in our recent work.[33] Using the Temkin isotherm, the evaluated dissociation constant K_D was 0.94 × 10^{-3} ng mL^{-1} ($R^2 = 0.991$) and 0.23 ng mL^{-1} ($R^2 = 0.962$) for SOL-Ty-nanoMIP and SP-Ty-nanoMIP sensors, respectively. From these results, it was evident that SOL-Ty-nanoMIPs have the best performance for integration into the sensor and the quantification of Ty. In addition, nanoMIPs produced *via* solid-phase imprinting are typically larger in size compared with solution nanoMIPs. This translates into a much higher binding site density on the surface of the electrode for the SOL nanoMIPs, which helps in driving the sensor performance. Therefore, the SOL-Ty-nanoMIPs and their counterpart nanoNIPs have been selected for the sensor preparation and further optimisation and characterisation studies.

3.3 Optimisation of sensor preparation

Taguchi experimental design was used to find the optimal conditions for sensor preparation. For this, the parameters including the time of chronoamperometric deposition to obtain the TA-SAM on SPAuE, the nanoMIP (and nanoNIP) immobilisation time, and the Ty-nanoMIP/nanoNIP loading time to interact with Ty were studied through Taguchi L9 orthogonal array design. We fixed the nanoMIP concentration at 0.25 mg mL^{-1}. In fact, we assume that a lower concentration of nanoMIPs for the immobilisation process can be beneficial as it can prevent excessive deposition and subsequent steric hindering effects during Ty binding.[36]

S/N ratios have been calculated according to the criterion "Larger is better", and reported in Table S2 in the ESI,† where the highest S/N ratio defines the optimum level of that factor. At the same time, the contribution of parameters to the response can be determined by comparing the calculated max–min (Δ) values for each parameter in the response table for S/N (Table S3 in the ESI†). A high Δ value means more effective contribution to the response variation, which resulted in the order $X_3 > X_2 > X_1$, where X_3 was the time of incubation of trypsin solution onto Ty-nanoMIPs/nanoNIPs. The computed S/N ratio in Fig. S6 in the ESI† shows that the optimal conditions were as follows: 2100 s of CA measurement, 30 min for nanoMIP/nanoNIP immobilisation, and 10 min of sensor loading time in 3 ng mL^{-1} of Ty dissolved in ammonium acetate buffer as the supporting electrolyte. Interestingly, increasing the time of nanoparticle immobilisation causes a decrease in sensor performance, possibly due to aggregation of the nanoparticles onto the electrode surface or deposition above a certain level where steric effects can become apparent. The effect of CA measurement is directly correlated to the TA-SAM layer covering the SPAuE, that is being activated to promote nanoparticle immobilisation. The results show that 2100 s during CA measurements can be used to control the functionalisation step, leading to produce a controlled functionalised layer on the SPAuE.

3.4 Analytical performances of the optimised sensor

The analytical performances of sensors have been evaluated by the exposure of varying concentrations of trypsin ranging from 3 to 46 ng mL^{-1}, dissolved in ammonium acetate buffer solution (pH = 6). EIS spectra were recorded and compared with those obtained for nanoNIPs (Fig. 2).

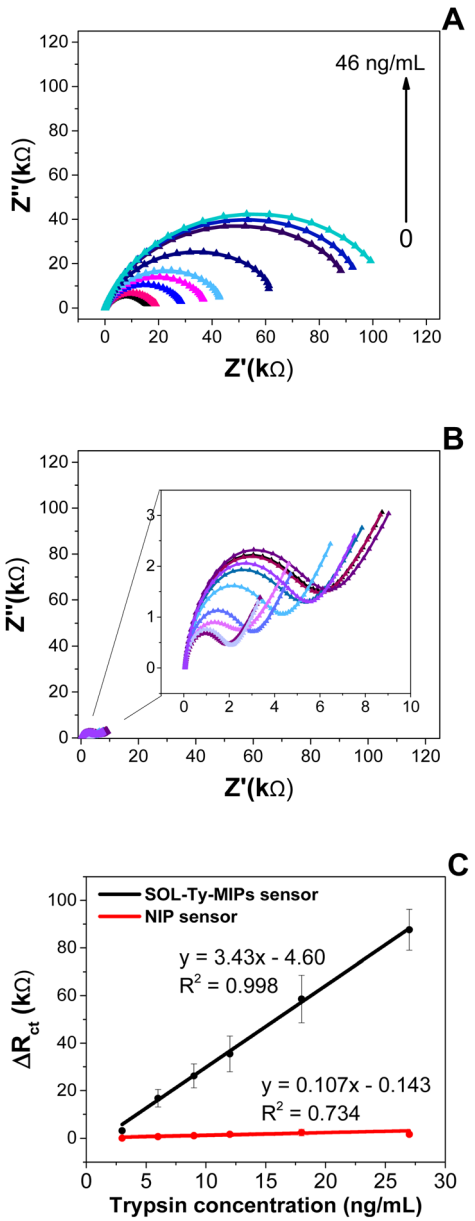

Fig. 2 Nyquist plots for (A) SOL-Ty-MIP and (B) NIP sensors obtained after exposure to 3, 6, 9, 12, 18, 27 ng mL^{-1} of Ty dissolved in ammonium acetate buffer (50 mM, pH = 6), and (C) related calibration plots.

EIS measurements were also applied in the case of bare SPAuE and TA-SAM/SPAuE (see Section 7 in the ESI†). Comparison to that obtained for bare SPAuE and TA-SAM/SPAuE confirmed the goodness of the imprinting process and the subsequent high-correlated sensor responses. As shown in Fig. 2, the sensor exhibited high imprinted quality properties compared to the NIP-based sensor. In particular, the optimised SOL-Ty-nanoMIP sensor revealed a linear working range between 3 and 27 ng mL^{-1} of Ty concentration, whereas NIP sensors do not exhibit a proportional correlation within the same tested concentration. Hence, the imprinted nanoparticles were 30 times more sensitive than the

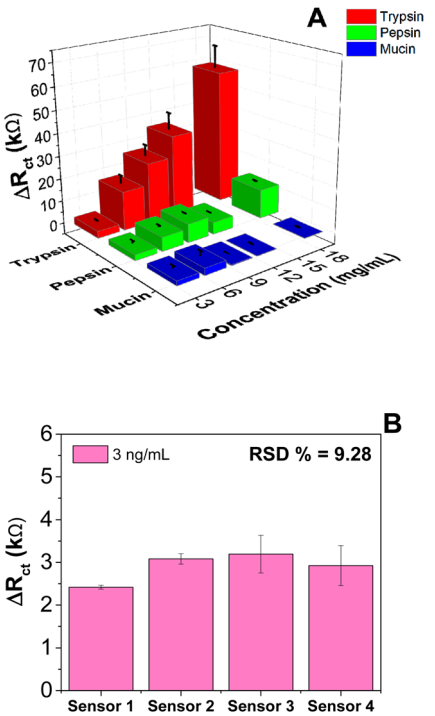

Fig. 3 (A) Cross-reactivity tests on SOL-Ty-nanoMIP sensors against pepsin and mucin, respectively, as structural interferents, compared with that observed for trypsin. (B) Reproducibility tests on the sensor done at 3 ng mL^{-1} of Ty.

respective NIPs, confirming the preparation of a highly sensitive receptor for Ty quantification, with a LOD of 1.06 ± 0.5 ng mL^{-1}.

3.5 Selectivity and reproducibility studies of the SOL-Ty-nanoMIP sensor

In addition to sensitivity, the selectivity of the SOL-Ty-nanoMIP sensor against potential interferences is a key parameter for sensor development. In this respect, pepsin and mucin[37] were selected as co-existing salivary proteins, which can potentially interfere with Ty.[38] The solutions containing the respective interferents were prepared in the same range of concentration for Ty detection, and sensor responses were recorded and compared (Fig. 3A). EIS data acquired for the competitive proteins are reported in Fig. S8 (in the ESI†). In the case of both competitive protein detection, the SOL-Ty-nanoMIP sensor shows a low non-specific response.

It can be clearly deduced that the imprinting process imparts recognition memory and specificity for Ty molecules, and this results in a sensor suitable for selective recognition of Ty. Fig. 3B summarises the reproducibility of sensor responses after exposure to a fixed concentration of Ty (3 ng mL^{-1}). The relative standard deviation (% RSD) of four different sensors was 9.28%, representing the sensor inter-batch precision. The repeatability of the sensor was also assessed by consecutive EIS measurements at the same Ty concentration, revealing a RSD of 5%; this indicates good sensor stability and robustness of the manufacturing process.

Table 1 Analytical performances of recently developed sensors based on MIPs for the determination of trypsin[a]

Sensor configuration	MIP film[1]	NIR CDs/ZIF-8/MIP[1]	MIP film[2]	NanoMIP film[1]	NanoMIP film[3]
Preparation method	Photopolymerisation and spin coating	Sol–gel polymerisation	Microcontact imprinting	Miniemulsion polymerisation	Liquid phase polymerisation
Sensing principle	Piezoelectric sensor	Fluorescent sensor	Capacitive biosensor	Piezoelectric sensor	Impedimetric sensor
LOD (ng mL^{-1})	25.33	8.8×10^{-6}	7.2×10^{-3}	70	1.06
Analytical range (ng mL^{-1})	6–60	5×10^{-5} to 9×10^{-2}	2.4×10^{-3} to 2400	125–2000	3–46
Imprinting factor	4.5	2.84	N.R.	N.R.	34
Reference	39	40	41	42	This work

[a] NIR CDs: near infrared fluorescent carbon dots; ZIF-8: zeolite imidazole framework-8. Transduction: [1]gold coated quartz crystal electrode; [2]gold electrode; [3]screen-printed gold electrode (SPAuE).

Table 2 Recovery studies on spiked artificial saliva

Added value (ng mL^{-1})	Found value (ng mL^{-1})	[a]Error, ±	Recovery (%)
9	9.66	$\pm 10^{-3}$	107.4
12	12.39	$\pm 10^{-4}$	103.3

[a] $n = 3$.

To further investigate the performances of the proposed sensor, the results obtained were compared with other methods as presented in Table 1.

It can be seen that the proposed sensor exhibits the lowest LOD, with a setup that is easy to produce and with short response times. In addition, the SOL-Ty-nanoMIPs were prepared using a simple, rapid and eco-friendly synthetic procedure which uses water as the solvent.

3.6 Proof-of-application in artificial spiked saliva

Considering the promising performances in standard solution of PBS, we checked the applicability of the optimised SOL-Ty-nanoMIP sensor in artificial spiked saliva as a proof-of-application in complex biological matrices. The obtained recovery percentage (%) for $n = 3$ measurements (Table 2) between 103 and 107% demonstrated great potential for practical application in the non-invasive assessment of Ty for clinical applications.

4. Conclusions

In this work, we described the preparation of an innovative sensor device based on nanosized molecularly imprinted polymers (nanoMIPs) for the quantification of Ty. Both nanoMIPs by solid-phase (SP-nanoMIPs) and liquid-phase (SOL-nanoMIPs) imprinting had high sensitivity towards the target analyte. Even if the solid-phase approach resulted in nanoMIPs with lower K_D (as determined by SPR), in the current setup SOL-nanoMIPs proved more appropriate. Taguchi design optimisation allowed for the preparation of a new high-performance sensor based on SOL-nanoMIPs for the detection of Ty in solution. Selectivity tests against potential interferents, *e.g.* mucin and pepsin, confirmed the selectivity of the nanoMIP towards Ty. Finally, the presented sensor could be easily proposed for the detection of Ty in complex matrices.

Conflicts of interest

There are no conflicts to declare.

Acknowledgements

The authors would like to acknowledge the financial support of the MIUR-Progetti di Ricerca di Rilevante Interesse Nazionale (PRIN) (Bando PRIN 2022, Prot. P2022T3HFA), and PhD program entitled "Green analytical chemistry: development of molecularly imprinted polymers for emerging pollutants" (CUP: F85F21005750001) funded by "Dottorati su tematiche Green del PON R&I 2014–2020".

References

1 Y.-J. Wang, X.-Q. Lang, D. Wu, Y.-Q. He, C.-H. Lan, B. Wang, *et al.*, Salivary pepsin as an intrinsic marker for diagnosis of sub-types of gastroesophageal reflux disease and gastroesophageal reflux disease-related disorders, *J. Neurogastroenterol. Motil.*, 2020, **26**(1), 74.
2 B. P. Crulhas, C. R. Basso, G. R. Castro and V. A. Pedrosa, Recent advances based on a sensor for cancer biomarker detection, *ECS J. Solid State Sci. Technol.*, 2021, **10**(4), 047004.
3 WHO, *World Health Organization Statistical Information System, WHO Mortality Database*, 2015.
4 O. Deutsch, Y. Haviv, G. Krief, N. Keshet, R. Westreich, S. Stemmer, *et al.*, Possible proteomic biomarkers for the detection of pancreatic cancer in oral fluids, *Sci. Rep.*, 2020, **10**(1), 1–13.
5 X. Lin, Z. Zhu, C. Zhao, S. Li, Q. Liu, A. Liu, *et al.*, Robust oxidase mimicking activity of protamine-stabilized platinum nanoparticles units and applied for colorimetric sensor of trypsin and inhibitor, *Sens. Actuators, B*, 2019, **284**, 346–353.
6 C.-Y. Poon, Q. Li, J. Zhang, Z. Li, C. Dong, A. W.-M. Lee, *et al.*, FRET-based modified graphene quantum dots for direct trypsin quantification in urine, *Anal. Chim. Acta*, 2016, **917**, 64–70.

7 T. Xia, Q. Ma, T. Hu and X. Su, A novel magnetic/photoluminescence bifunctional nanohybrid for the determination of trypsin, *Talanta*, 2017, **170**, 286–290.
8 E. González-Fernández, N. Avlonitis, A. F. Murray, A. R. Mount and M. Bradley, Methylene blue not ferrocene: optimal reporters for electrochemical detection of protease activity, *Biosens. Bioelectron.*, 2016, **84**, 82–88.
9 A. McGuigan, P. Kelly, R. C. Turkington, C. Jones, H. G. Coleman and R. S. McCain, Pancreatic cancer: a review of clinical diagnosis, epidemiology, treatment and outcomes, *World J. Gastroenterol.*, 2018, **24**(43), 4846.
10 J. Loo, W. Yan, P. Ramachandran and D. Wong, Comparative human salivary and plasma proteomes, *J. Dent. Res.*, 2010, **89**(10), 1016–1023.
11 H. Sohrabi, N. Bolandi, A. Hemmati, S. Eyvazi, S. Ghasemzadeh, B. Baradaran, *et al.*, State-of-the-art cancer biomarker detection by portable (bio) sensing technology: a critical review, *Microchem. J.*, 2022, 107248.
12 P. S. Gaikwad and R. Banerjee, Advances in point-of-care diagnostic devices in cancers, *Analyst*, 2018, **143**(6), 1326–1348.
13 S. A. Piletsky and A. P. Turner, Electrochemical sensors based on molecularly imprinted polymers, *Electroanalysis*, 2002, **14**(5), 317–323.
14 M. J. Whitcombe, I. Chianella, L. Larcombe, S. A. Piletsky, J. Noble, R. Porter, *et al.*, The rational development of molecularly imprinted polymer-based sensors for protein detection, *Chem. Soc. Rev.*, 2011, **40**(3), 1547–1571.
15 N. Leibl, K. Haupt, C. Gonzato and L. Duma, Molecularly imprinted polymers for chemical sensing: a tutorial review, *Chemosensors*, 2021, **9**(6), 123.
16 W. Kutner and P. S. Sharma, *Molecularly Imprinted Polymers for Analytical Chemistry Applications*, Royal Society of Chemistry, 2018.
17 C. Malitesta, E. Mazzotta, R. A. Picca, A. Poma, I. Chianella and S. A. Piletsky, MIP sensors-the electrochemical approach, *Anal. Bioanal. Chem.*, 2012, **402**, 1827–1846.
18 A. G. Cruz, I. Haq, T. Cowen, S. Di Masi, S. Trivedi, K. Alanazi, *et al.*, Design and fabrication of a smart sensor using *in silico* epitope mapping and electro-responsive imprinted polymer nanoparticles for determination of insulin levels in human plasma, *Biosens. Bioelectron.*, 2020, **169**, 112536.
19 K. Alanazi, A. G. Cruz, S. Di Masi, A. Voorhaar, O. S. Ahmad, T. Cowen, *et al.*, Disposable paracetamol sensor based on electroactive molecularly imprinted polymer nanoparticles for plasma monitoring, *Sens. Actuators, B*, 2021, **329**, 129128.
20 I. Haq, A. G. Cruz, S. Di Masi, T. Cowen, N. S. Allcock, C. Malitesta, *et al.*, Smart nano-actuators for electrochemical sensing of Metformin in human plasma, *Sens. Actuators, B*, 2023, **376**, 132928.
21 I. E. Tothill and M. Abdin, Nano molecular imprinted polymers (nanoMIPs) for food diagnostics and sensor, *Nanotechnology: Food and Environmental Paradigm*. 2017, pp. 131–151.
22 K. G. Shevchenko, I. S. Garkushina, F. Canfarotta, S. A. Piletsky and N. Barlev, Nano-molecularly imprinted polymers (nanoMIPs) as a novel approach to targeted drug delivery in nanomedicine, *RSC Adv.*, 2022, **12**(7), 3957–3968.
23 M. Akram, M. C. Stuart and D. K. Wong, Direct application strategy to immobilise a thioctic acid self-assembled monolayer on a gold electrode, *Anal. Chim. Acta*, 2004, **504**(2), 243–251.
24 S. Dong and J. Li, Self-assembled monolayers of thiols on gold electrodes for bioelectrochemistry and biosensors, *Bioelectrochem. Bioenerg.*, 1997, **42**(1), 7–13.
25 G. Ziyatdinova, T. Antonova, V. Vorobev, Y. Osin and H. Budnikov, Selective voltammetric determination of α-lipoic acid on the electrode modified with SnO_2 nanoparticles and cetyltriphenylphosphonium bromide, *Monatsh. Chem.*, 2019, **150**, 401–410.
26 R. Sahli, C. Fave, N. Raouafi, K. Boujlel, B. Schöllhorn and B. Limoges, Switching on/off the chemisorption of thioctic-based self-assembled monolayers on gold by applying a moderate cathodic/anodic potential, *Langmuir*, 2013, **29**(17), 5360–5368.
27 E. M. Dief and N. Darwish, Electrochemically Fabricated Molecule–Electrode Contacts for Molecular Electronics, *Curr. Opin. Electrochem.*, 2022, 101019.
28 L. Cenci, E. Andreetto, A. Vestri, M. Bovi, M. Barozzi, E. Iacob, *et al.*, Surface plasmon resonance based on molecularly imprinted nanoparticles for the picomolar detection of the iron regulating hormone Hepcidin-25, *J. Nanobiotechnol.*, 2015, **13**, 1–15.
29 A. Poma, A. Guerreiro, M. J. Whitcombe, E. V. Piletska, A. P. Turner and S. A. Piletsky, Solid-phase synthesis of molecularly imprinted polymer nanoparticles with a reusable template–"plastic antibodies", *Adv. Funct. Mater.*, 2013, **23**(22), 2821–2827.
30 L. Cenci, M. Bertolla, A. Anesi, E. Ambrosi, G. Guella and A. M. Bossi, Micro-versus nano-sized molecularly imprinted polymers in MALDI-TOF mass spectrometry analysis of peptides, *Anal. Bioanal. Chem.*, 2017, **409**, 6253–6261.
31 F. Canfarotta, J. Czulak, A. Guerreiro, A. G. Cruz, S. Piletsky, G. E. Bergdahl, *et al.*, A novel capacitive sensor based on molecularly imprinted nanoparticles as recognition elements, *Biosens. Bioelectron.*, 2018, **120**, 108–114.
32 X. Sánchez-Sánchez, A. Elias-Zuñiga and M. Hernández-Avila, Processing of ultra-high molecular weight polyethylene/graphite composites by ultrasonic injection moulding: Taguchi optimization, *Ultrason. Sonochem.*, 2018, **44**, 350–358.
33 M. Costa, S. Di Masi, A. Garcia-Cruz, S. A. Piletsky and C. Malitesta, Disposable electrochemical sensor based on ion imprinted polymeric receptor for Cd (II) ion monitoring in waters, *Sens. Actuators, B*, 2023, **383**, 133559.
34 J. B. Claver, M. V. Mirón and L. Capitán-Vallvey, Disposable electrochemiluminescent biosensor for lactate determination in saliva, *Analyst*, 2009, **134**(7), 1423–1432.
35 J. Kim, S. Imani, W. R. de Araujo, J. Warchall, G. Valdés-Ramírez, T. R. Paixão, *et al.*, Wearable salivary uric acid mouthguard biosensor with integrated wireless electronics, *Biosens. Bioelectron.*, 2015, **74**, 1061–1068.

36 G. Sener, L. Uzun, R. Say and A. Denizli, Use of molecular imprinted nanoparticles as biorecognition element on surface plasmon resonance sensor, *Sens. Actuators, B*, 2011, **160**(1), 791–799.
37 H. Temiz, U. Aykut, E. Okumus and S. Turhan, The partial purification and properties of pepsin obtained from turkey proventriculus, *Biotechnol. Bioprocess Eng.*, 2007, **12**, 450–456.
38 H. Singh and A. Sarkar, Behaviour of protein-stabilised emulsions under various physiological conditions, *Adv. Colloid Interface Sci.*, 2011, **165**(1), 47–57.
39 J. W. Byeon, J. C. Yang, C. H. Cho, S. J. Lim, J. P. Park and J. Park, A Facile surface-imprinting strategy for trypsin-imprinted polymeric chemosensors using two-step spin-coating, *Chemosensors*, 2023, **11**(3), 189.
40 S. Chen, J. Fu, S. Zhou, X. Wu, S. Tang and P. Zhao, An eco-friendly near infrared fluorescence molecularly imprinted sensor based on zeolite imidazolate framework-8 for rapid determination of trace trypsin, *Microchem. J.*, 2021, **168**, 106449.
41 G. Ertürk, M. Hedström and B. Mattiasson, A sensitive and real-time assay of trypsin by using molecular imprinting-based capacitive biosensor, *Biosens. Bioelectron.*, 2016, **86**, 557–565.
42 N. A. Karaseva, B. Pluhar, E. A. Beliaeva, T. N. Ermolaeva and B. Mizaikoff, Synthesis and application of molecularly imprinted polymers for trypsin piezoelectric sensors, *Sens. Actuators, B*, 2019, **280**, 272–279.

